Forschung im Ingenieurwesen (2023) 87:1081–1094
https://doi.org/10.1007/s10010-023-00707-1

ORIGINALARBEITEN/ORIGINALS

Improvement of the transmission efficiency in electric vehicles by using double staggered helical gears with shortened teeth

Ignacio Gonzalez-Perez[1] · Alfonso Fuentes-Aznar[2]

Received: 11 March 2023 / Accepted: 2 August 2023 / Published online: 13 September 2023

Abstract

The application of double staggered helical gears with shortened teeth is proposed to increase the efficiency of gear reducers applied in electric vehicles. The staggered helical gears are designed with short addendum and dedendum as well as a phase angle between their two parts. Reduction of power losses is achieved by avoiding contact between tooth surfaces where the sliding velocities are larger, since the meshing occurs in areas close to the pitch circle during a longer period of the cycle of meshing. The calculation of the efficiency is based on the application of the finite element method through two algorithms for post-processing the obtained results. The first one is based on the use of tangential forces and sliding velocities to compute the power losses along the cycle of meshing. The second one is based on the determination of the input and output powers through the torques and velocities at the pinion and gear reference nodes of the finite element model. A constant friction coefficient is being considered between the contacting tooth surfaces for all the geometries. Several two-stage gear transmissions are analyzed and compared, considering standard helical gears and their counterpart double staggered helical gears with shortened teeth, different facewidth-to-module ratios, and different helix angles. The results show an improvement in the efficiency about 1.8 percentile points among the compared geometries.

✉ Ignacio Gonzalez-Perez
ignacio.gonzalez@upct.es

Alfonso Fuentes-Aznar
afeme@rit.edu

[1] Department of Mechanical Engineering, Materials and Manufacturing, Universidad Politecnica de Cartagena, Dr. Fleming s/n, 30202 Cartagena, Spain

[2] Department of Mechanical Engineering, Rochester Institute of Technology, 76 Lomb Memorial Drive, Rochester, 14623, USA

Verbesserung der Übertragungseffizienz in Elektrofahrzeugen durch den Einsatz von doppelt versetzten Schrägverzahnungen mit verkürzten Zähnen

Zusammenfassung

Der Einsatz von doppelt versetzten Schrägverzahnungen mit verkürzten Zähnen wird vorgeschlagen, um die Effizienz von Getrieben in Elektrofahrzeugen zu steigern. Die Schrägstirnräder sind mit kurzer Kopf- und Fußhöhe sowie einem Phasenwinkel zwischen ihren beiden Teilen entworfen. Die Reduzierung von Leistungsverlusten wird dadurch erreicht, dass der Kontakt zwischen Zahnoberflächen vermieden wird, an denen die Gleitgeschwindigkeiten größer sind, da der Eingriff während eines längeren Zeitraums des Eingriffszyklus in Bereichen nahe dem Teilkreis erfolgt. Die Berechnung der Effizienz basiert auf der Anwendung der Finite-Elemente-Methode durch zwei Algorithmen zur Nachbearbeitung der erhaltenen Ergebnisse. Die erste basiert auf der Nutzung von Tangentialkräften und Gleitgeschwindigkeiten zur Berechnung der Leistungsverluste entlang des Eingriffszyklus. Die zweite basiert auf der Bestimmung der Eingangs- und Ausgangsleistungen anhand der Drehmomente und Geschwindigkeiten an den Ritzel- und Zahnrad-Referenzknoten des Finite-Elemente-Modells. Für alle Geometrien wird ein konstanter Reibungskoeffizient, zwischen den sich berührenden Zahnoberflächen berücksichtigt. Mehrere zweistufige Zahnradgetriebe werden analysiert und verglichen, unter Berücksichtigung von Standard-Schrägverzahnungen und ihren Gegenstücken mit doppelt versetzten Schrägverzahnungen mit verkürzten Zähnen, unterschiedlichen Verhältnissen von Zahnbreite zu Modul und unterschiedlichen Schrägungswinkeln. Die Ergebnisse zeigen eine Verbesserung der Effizienz um etwa 1,8 Prozentpunkte zwischen den verglichenen Geometrien.

1 Introduction

Electric vehicles require transmissions with high efficiency, low levels of noise and vibration and high power density [1]. Nowadays, there is an area of research directed to get low-loss gears. These gears present macro-geometrical modifications that allow power losses due to sliding friction to be reduced, since they concentrate sliding close to the pitch point. Such gear drives are featured with small modules, high pressure angles, and small transverse contact ratios. In [2], low-loss gears are analyzed in planetary gearboxes by an analytical-numerical approach to estimate the power losses. In [3], a new type of profile for spur gears is proposed to reduce the sliding and the power losses. In [4], a method for modeling elasto-hydrodynamically lubricated contacts is applied to low-loss gear drives to show that the effect of low-loss geometry is very small in the overall frictional losses.

On the other hand, there has been an intensive research directed to get an accurate prediction of the friction coefficient and consequently of the power losses in gear drives. To this end, in [5], a computational model is proposed as a combination of a load distribution model, a friction model based on an elasto-hydrodynamic behavior and a mechanical efficiency formulation. A similar study is applied in [6] to spiral bevel gear pairs. In [7], the influence of the addendum modification in the efficiency of spur gear pairs is investigated using two approaches of friction coefficient calculation, considering a mean friction coefficient and a variable friction coefficient with elasto-hydrodynamic considerations, suggesting the use of the first one for optimization purposes. In [8], power losses were predicted in cylindrical gears through an accurate prediction of the friction coefficient taking into account as well elasto-hydrodynamic conditions.

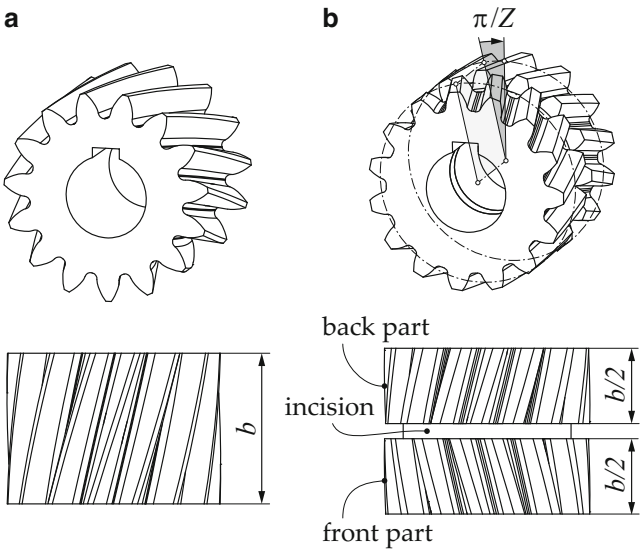

Fig. 1 Standard helical gear and double staggered helical gear with shortened teeth

In this paper, the use of double staggered helical gears with short addendum and dedendum is proposed to be applied in a two-stage gear transmission of an electric vehicle. Fig. 1a shows a standard helical gear and Fig. 1b shows its counterpart as a double staggered helical gear with shortened teeth. The latter has two parts, the front and back ones, separated by the incision part. The incision part is required to avoid interference with the cutting tool during the manufacturing of each part. The total facewidth b of these two parts is the same as in the standard helical gear. There is a phase angle π/Z between these two parts, be-

ing Z the number of teeth. The phase angle allows the transverse contact ratio to be increased. As a consequence, the gear addendum and dedendum can be reduced in order to get a similar transverse contact ratio to standard helical gear drive. This is the main idea to avoid areas of meshing far away from the pitch cylinder and reduce the amount of power losses due to frictional energy.

The amount of load-dependent power losses due to friction will be compared in several gear geometries of standard helical gears and their counterpart double staggered helical gears with shortened teeth, considering facewidth-to-module ratios $b/m \approx 12$ and $b/m \approx 20$, and helix angles 7.5° and 15°.

The finite element method is applied to the determination of the frictional energy and the efficiency of the gear transmission. The approach is based on the work [9] and determines the loss energy from the sliding velocities and the tangential forces at the nodes of the deformed finite element model. An alternative approach based on the determination of the input and output powers using magnitudes associated to the pinion and gear reference nodes (velocity and torque) is also presented. The advantage of these approaches is that no assumptions about the formation of the bearing contact under load are required and that the actual geometries of the tooth surfaces under load are considered in the analysis.

In all the analyses, a constant friction coefficient is assumed. The goal here is to highlight and compare the effects of the considered low-loss geometries in the power losses for the same value of the friction coefficient, assuming that the differences with the analyses using a non-constant friction coefficient should be low, as it can be drawn from previous studies [7].

2 Gear geometry

Gear tooth surfaces are generated as envelopes to the family of cutter tooth surfaces in a coordinate system that is rigidly connected to the gear [10]. Fig. 2a shows the generation of a standard helical gear by a rack-cutter and Fig. 2b and 2c show the generation of a double staggered helical gear using two rack cutters for each part. Each part is generated independently. Coordinate system S_g is rigidly connected to the gear whereas coordinate system S_c is rigidly con-

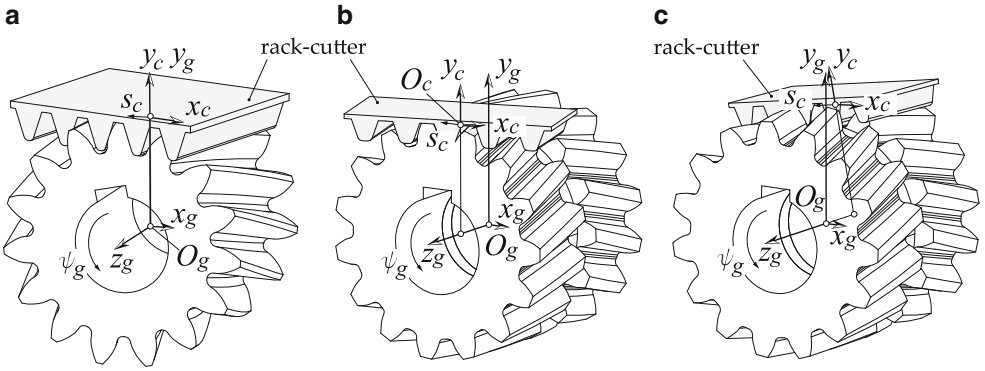

Fig. 2 Generation of a standard and a double staggered helical gear

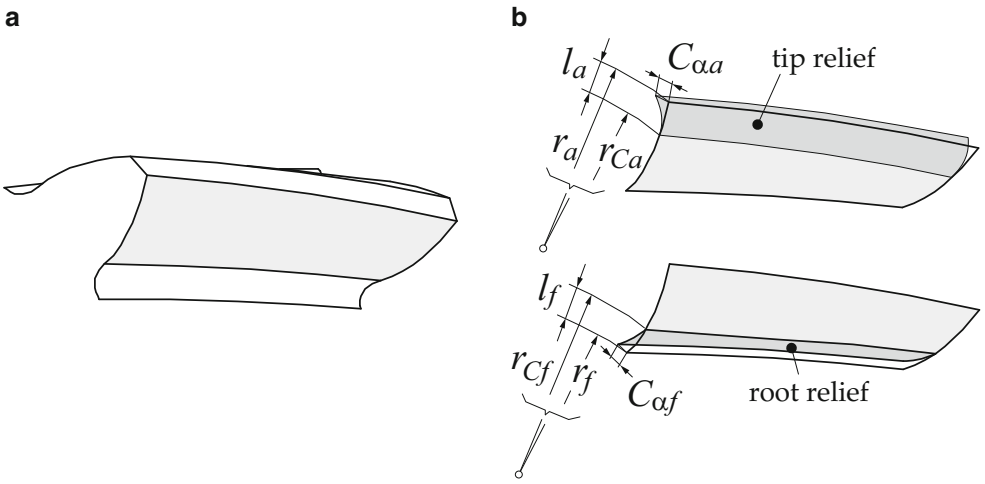

Fig. 3 For illustration of tip and root reliefs: **a** generated tooth surface, **b** interpolated tooth surfaces with profile tip relief and profile root relief modifications

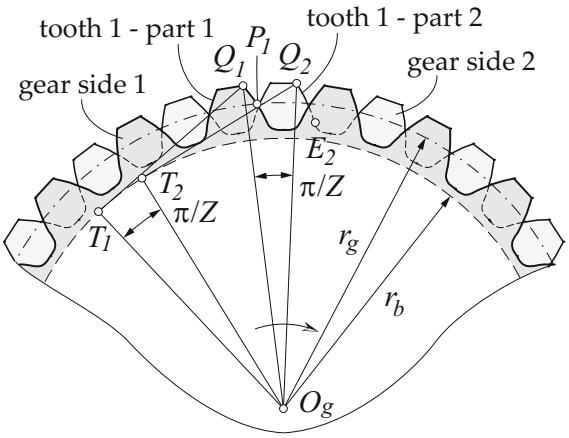

Fig. 4 Double staggered gear with shortened teeth

nected to the rack-cutter. Rotation ψ_g of the gear is related to the translation s_c of the cutter through the relation

$$\psi_g = \frac{s_c}{r_g} \tag{1}$$

where r_g is the gear pitch radius.

Gear tooth surfaces are then interpolated by B-Splines surfaces [11] that can be modified through linear or parabolic functions. In this paper, parabolic tip and root reliefs will be applied in all the compared geometries to avoid edge contacts along the cycle of meshing. Two parameters are defined for each relief: the datum length l_a and amount $C_{\alpha a}$ of tip relief and datum length l_f and amount $C_{\alpha f}$ of root relief (see Fig. 3). The datum length l_a is defined as a radial distance between the addendum circle with radius r_a and the datum circle with radius r_{Ca}. The datum length l_f is defined similarly as a radial distance between the circle with form radius r_f and the datum circle with radius r_{Cf}. Tip and root relief will be applied to the pinion. A similar effect avoiding edge contacts could be found by substituting the pinion root relief by a gear tip relief.

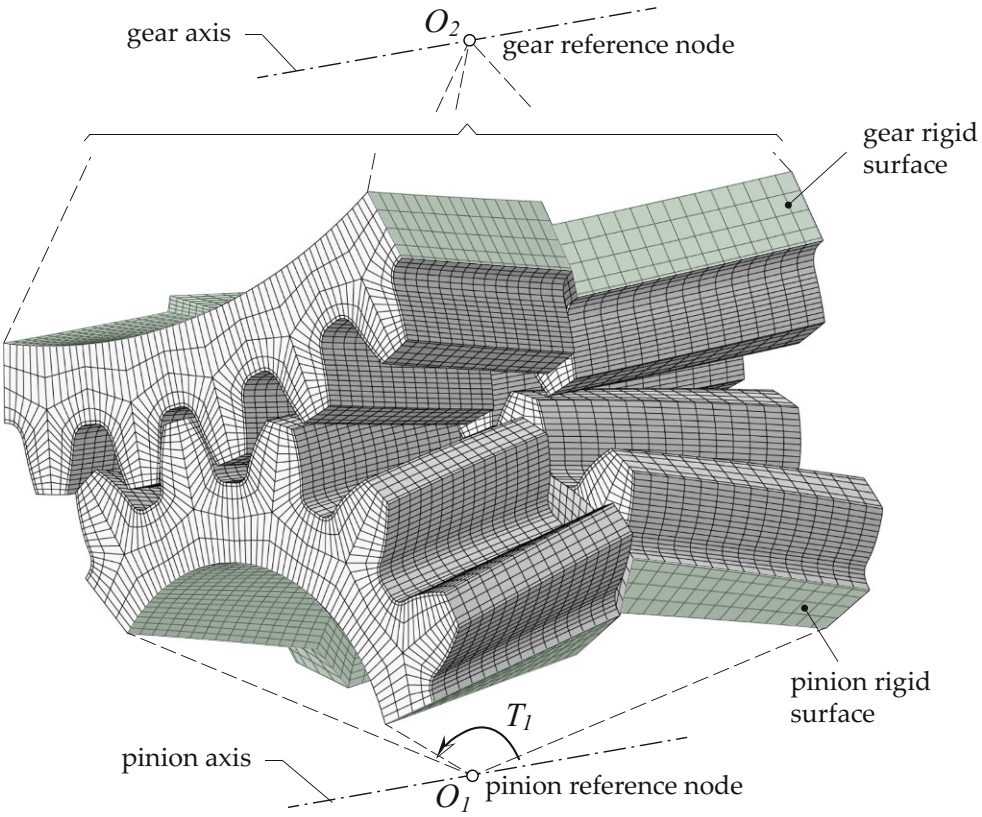

Fig. 5 Finite element model of a gear drive with double staggered helical gears

3 Transverse contact ratio in double staggered helical gear drives

In the case of a standard helical gear drive, the transverse contact ratio can be obtained as a function of the addendum coefficient a as

$$\varepsilon_{\alpha,s}(a) = \frac{1}{2\pi}\left[Z_1\sqrt{\left(\frac{r_{a1}(a)}{r_{b1}}\right)^2 - 1} + Z_2\sqrt{\left(\frac{r_{a2}(a)}{r_{b2}}\right)^2 - 1} - (Z_1 + Z_2)\tan\alpha_t \right] \tag{2}$$

Here, Z_1 and Z_2 are the gear tooth numbers, r_{a1} and r_{a2} are the addendum radii, r_{b1} and r_{b2} are the base radii, and α_t is the working transverse pressure angle.

The value of the transverse contact ratio in a double staggered helical gear drive is increased respect to its coun-

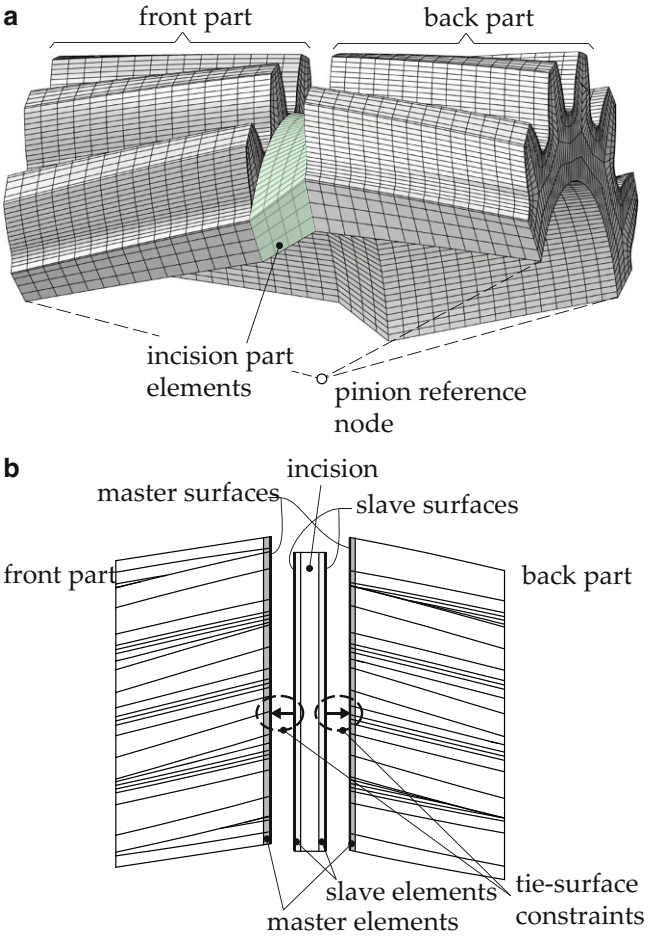

Fig. 6 **a** Finite element model of a double staggered helical pinion, and **b** schematic illustration of tie-surface constraints in the incision part

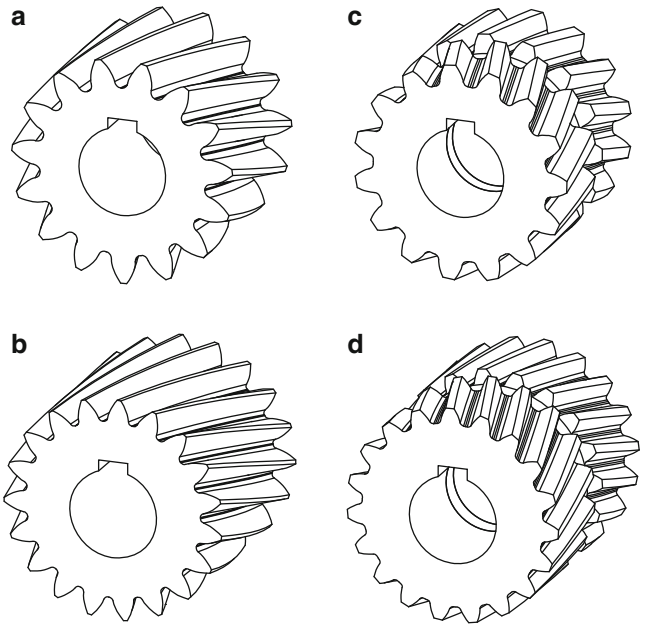

Fig. 7 Types of helical gear configurations: **a** single standard with $b/m \approx 12$, **b** single standard with $b/m \approx 20$, **c** double staggered with $b/m \approx 12$, and **d** double staggered with $b/m \approx 20$

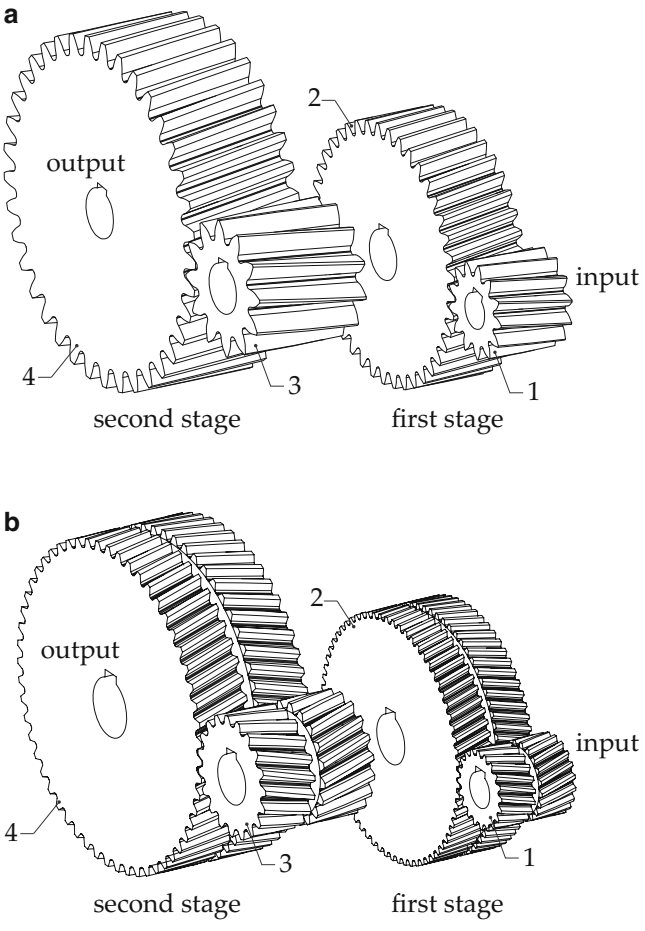

Fig. 8 **a** Transmission T1 ($b/m \approx 12$, $\beta = 7.5°$, with standard helical gears) and **b** transmission T8 ($b/m \approx 20$, $\beta = 15.0°$, with double staggered helical gears with shortened teeth)

Table 1 Variables of eight two-stage gear transmissions

Variable	T1	T2	T3	T4	T5	T6	T7	T8
Type[1]	S	S	D	D	S	S	D	D
Stage 1								
Module [mm]	3.0	2.0	3.0	2.0	2.5	1.75	2.5	1.75
Facewidth [mm]	40.0	42.0	40.0	42.0	35.0	38.0	35.0	38.0
Helix angle [°]	7.5	7.5	7.5	7.5	15.0	15.0	15.0	15.0
Center distance [mm]	83.5	87.5	83.5	87.5	79.5	79.5	79.5	79.5
ε_α	1.4	1.543	1.5	1.5	1.548	1.495	1.5	1.5
Pinion								
Tooth number	13	20	13	20	15	20	15	20
Addendum coef.	1.0	1.0	0.691	0.628	1.0	1.0	0.621	0.649
Dedendum coef.	1.25	1.25	0.941	0.878	1.25	1.25	0.871	0.899
Profile shift coef.	0.502	0.385	0.502	0.385	0.240	0.374	0.24	0.374
Gear								
Tooth number	41	66	41	66	47	67	47	67
Addendum coef.	1.0	1.0	0.691	0.628	1.0	1.0	0.621	0.649
Dedendum coef.	1.25	1.25	0.941	0.878	1.25	1.25	0.871	0.899
Profile shift coef.	0.144	0.006	0.144	0.006	−0.524	0.032	−0.524	0.032
Stage 2								
Module [mm]	4.5	3.0	4.5	3.0	3.5	2.75	3.5	2.75
Facewidth [mm]	60.0	62.0	60.0	62.0	45.0	56.0	45.0	56.0
Helix angle [°]	7.5	7.5	7.5	7.5	15.0	15.0	15.0	15.0
Center distance [mm]	112	115	112	115	110	109	110	109
ε_α	1.41	1.586	1.5	1.5	1.489	1.447	1.5	1.5
Pinion								
Tooth number	12	20	12	20	15	19	15	19
Addendum coef.	1.0	1.0	0.695	0.61	1.0	1.0	0.656	0.649
Dedendum coef.	1.25	1.25	0.945	0.86	1.25	1.25	0.906	0.899
Profile shift coef.	0.459	0.304	0.459	0.304	0.351	0.601	0.351	0.601
Gear								
Tooth number	37	56	37	56	46	55	46	55
Addendum coef.	1.0	1.0	0.695	0.61	1.0	1.0	0.656	0.649
Dedendum coef.	1.25	1.25	0.945	0.86	1.25	1.25	0.906	0.899
Profile shift coef.	−0.277	−0.298	−0.277	−0.298	−0.496	0.877	−0.496	0.877

[1] Type S: Standard helical, Type D: Double staggered helical with shortened teeth

terpart standard helical gear drive due to the applied angular offset between parts. Fig. 4 shows a double staggered gear that rotates clockwise. Due to the offset angle π/Z between parts 1 and 2 of each teeth, the contact length along the meshing line of a tooth pair is increased by $\pi r_b/Z$, being r_b the base radius. The mesh of tooth 1 starts at point E_2, that is in contact with a point of the addendum circle of the mating gear, and ends at point Q_1, but not at point Q_2. This consideration provides the following expression for the transverse contact ratio in a double staggered helical gear drive:

$$\varepsilon_{\alpha,d}(a) = \varepsilon_{\alpha,s}(a) + \frac{\pi r_b/Z}{2\pi r_b/Z} = \varepsilon_{\alpha,s}(a) + \frac{1}{2} \tag{3}$$

where $\varepsilon_{\alpha,s}(a)$ is obtained from Eq. (2).

The increased transverse contact ratio of double staggered gear drives allows the addendum and dedendum to be reduced in order to get a similar transverse contact ratio to its counterpart standard helical gear drive and at the same time avoid areas of meshing far from the pitch point where the sliding velocities are higher.

4 Finite element models

The finite element models are built following the ideas described in [10]. However, some new features are required for the models of double staggered helical gears. Fig. 5 shows a finite element model of a gear drive with double staggered helical gears with shortened teeth. A reduced

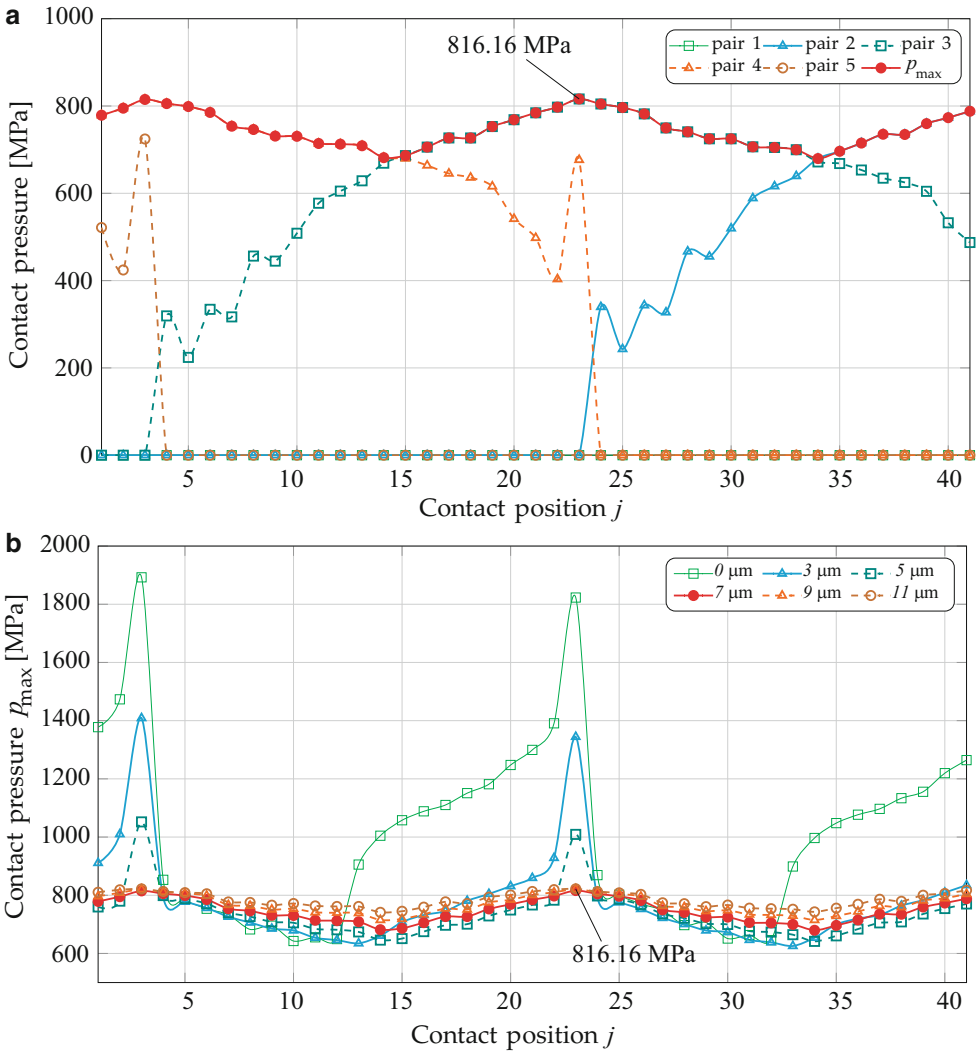

Fig. 9 Contact pressure at Stage 1 of transmission T1: **a** at each pair of contacting teeth when a tip-root relief $l_a = l_f = 1.5\,\text{mm}$ and $C_{\alpha a} = C_{\alpha f} = 7\,\mu\text{m}$ is considered, **b** comparison of p_{max} for different values of tip-root reliefs

Table 2 Optimized tip-root reliefs and maximum value of the optimized evolution of p_{max}

Variable	T1	T2	T3	T4	T5	T6	T7	T8
Stage 1								
T_1 [Nm]	137.0	137.0	137.0	137.0	137.0	137.0	137.0	137.0
n_1 [rpm]	4182.2	4182.2	4182.2	4182.2	4182.2	4182.2	4182.2	4182.2
$l_a = l_f$ [mm]	1.5	1.0	1.5	1.0	1.25	0.875	1.25	0.875
$C_{\alpha a} = C_{\alpha f}$ [µm]	7.0	5.0	7.0	7.0	9.0	5.0	9.0	9.0
Max. p_{max} [MPa]	816.1	871.3	1169.9	1206.2	1102.7	1033.1	1424.8	1380.6
Min. flank safety	1.593	1.492	1.111	1.078	1.179	1.258	0.912	0.942
Stage 2								
T_3 [Nm]	432.1	452.1	432.1	452.1	429.2	459.0	429.2	459.0
n_3 [rpm]	1326.0	1267.3	1326.0	1267.3	1334.9	1248.4	1334.9	1248.4
$l_a = l_f$ [mm]	2.25	1.5	2.25	1.5	1.75	1.375	1.75	1.375
$C_{\alpha a} = C_{\alpha f}$ [µm]	9.0	7.0	11.0	9.0	13.0	7.0	13.0	11.0
Max. p_{max} [MPa]	853.3	876.6	1201.6	1286.1	1101.2	1014.5	1562.1	1356.5
Min. flank safety	1.564	1.523	1.111	1.038	1.212	1.316	0.855	0.984

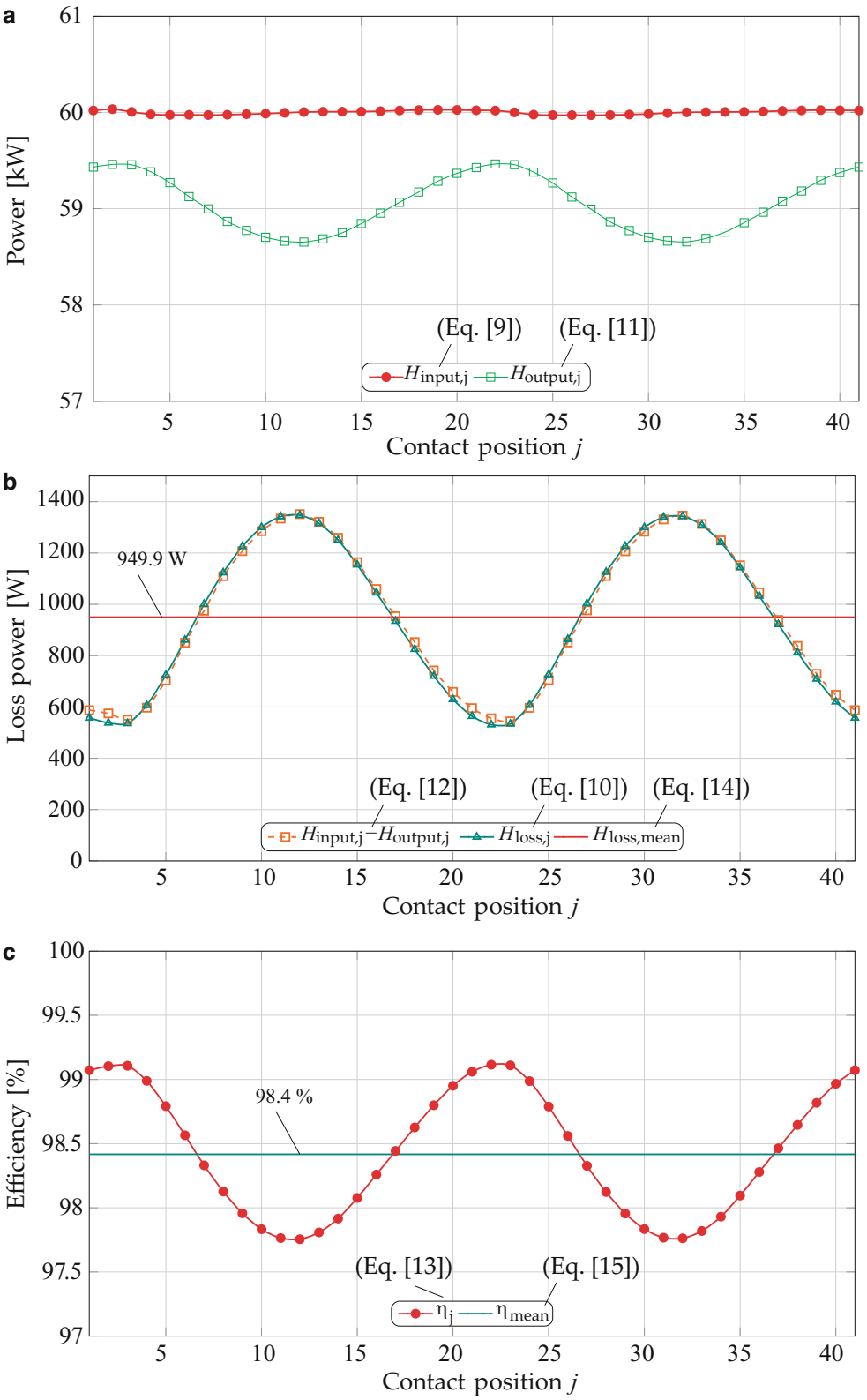

Fig. 10 Energy results for Stage 1 of transmission T1: **a** input and output powers, **b** power loss, and **c** efficiency

number of elements is illustrated in Fig. 5 for the purpose of clarity. The nodes on the bottom side and both end sides of the rim constitute a rigid surface. This includes the nodes of the bottom side of the incision (better illustrated in Fig. 6). The rigid surface is rigidly connected to the reference node defined at the axis of each gear. All the degrees of freedom are blocked at the reference nodes, but the rotation about the pinion axis is released at the pinion reference node.

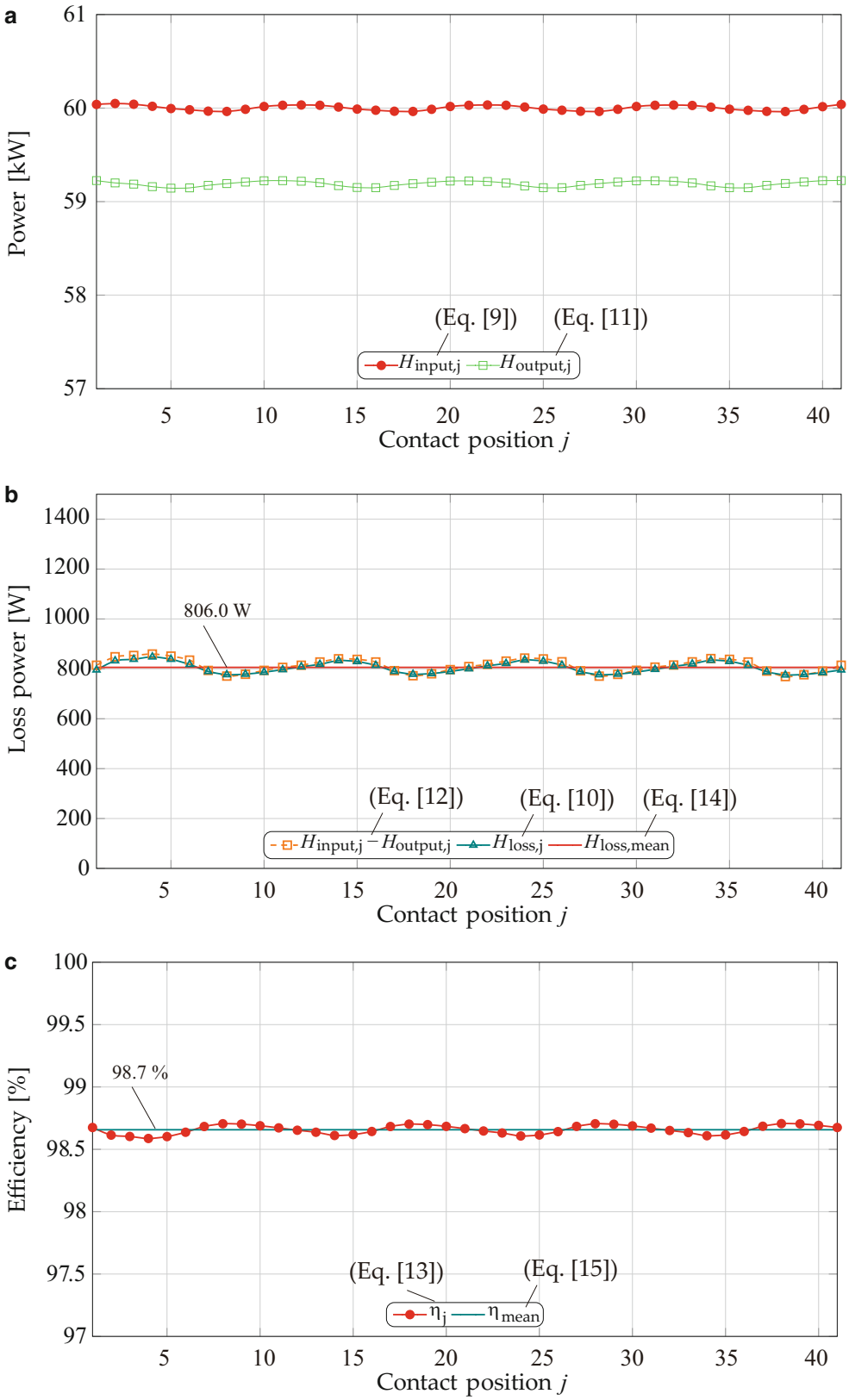

Fig. 11 Energy results for Stage 1 of transmission T3: **a** input and output powers, **b** power loss, and **c** efficiency

Table 3 Mean power losses and efficiencies

Variable	T1	T2	T3	T4	T5	T6	T7	T8
$H^{(1)}_{\text{loss,mean}}$ [W]	949.9	694.6	806.0	509.3	929.3	702.9	730.8	496.1
$\eta^{(1)}_{\text{mean}}$	0.9842	0.9884	0.9866	0.9915	0.9845	0.9883	0.9878	0.9917
$H^{(2)}_{\text{loss,mean}}$ [W]	1143.9	754.6	988.2	561.3	983.7	704.7	818.0	490.0
$\eta^{(2)}_{\text{mean}}$	0.9835	0.9874	0.9835	0.9906	0.9836	0.9883	0.9864	0.9918
$H_{\text{loss,mean}}$ [1]	2093.8	1449.2	1794.2	1070.6	1913.0	1407.6	1548.8	986.1
η_{mean} [2]	0.9654	0.9759	0.9703	0.9822	0.9683	0.9767	0.9744	0.9836

[1] $H_{\text{loss,mean}} = H^{(1)}_{\text{loss,mean}} + H^{(2)}_{\text{loss,mean}}$
[2] $\eta_{\text{mean}} = \eta^{(1)}_{\text{mean}} \cdot \eta^{(2)}_{\text{mean}}$

This allows an input torque T_1 to be applied at that degree of freedom. Several contact steps are considered to cover a cycle of meshing of $4\pi/Z_2$ radians of rotation of the gear. At each step, the rotation about the gear axis is released at its reference node, then this node is rotated a step angle, and after that it is blocked again, allowing the load to be applied.

Fig. 6a shows a better view of the incision elements in a double staggered helical pinion. The incision elements are joined to the front and back parts of the model using tie-surface constraints [12], which are schematically represented in Fig. 6b. Two element-based surfaces are created with some elements of the incision part (slave elements) and other two element-based surfaces are created with some elements of the front and back parts (master elements). These surfaces, slave and master, are tied as it is indicated in Fig. 6b.

5 Algorithm for determination of the efficiency

The algorithm is based on the computation of the frictional energy during the cycle of meshing. A constant friction coefficient μ, a reference input pinion velocity ω_1 and a constant input torque T_1 are assumed. The following steps are applied:

1. The reference output gear velocity ω_2 is determined as

$$\omega_2 = \omega_1 \frac{Z_1}{Z_2} \tag{4}$$

   where Z_1 and Z_2 are the tooth numbers of pinion and gear, respectively.
2. A cycle of meshing covering $4\pi/Z_2$ radians of rotation of the gear and divided into $n-1$ steps (n contact positions) is considered. Since the finite element analysis considers equally spaced step angles at the gear reference node along the cycle of meshing, the output gear velocity is considered as a constant value. The step time Δt is obtained then as

$$\Delta t = \left(\frac{4\pi}{Z_2}\frac{1}{n-1}\right)\frac{1}{\omega_2} \tag{5}$$

3. The input pinion velocity is computed at each contact position j, $j = \{0, ..., n-1\}$ from the field variable $\phi_{1,j}$ retrieved from the rotational degree of freedom of the pinion reference node. A central difference approximation is applied in contact positions $\{2, ..., n-3\}$ [13]

$$\omega_{1,j} = \frac{-\phi_{1,j+2} + 8\phi_{1,j+1} - 8\phi_{1,j-1} + \phi_{1,j-2}}{12\Delta t} \tag{6}$$

   A forward difference approximation is applied in contact positions {0,1}

$$\omega_{1,j} = \frac{-\phi_{1,j+2} + 4\phi_{1,j+1} - 3\phi_{1,j}}{2\Delta t} \tag{7}$$

   A backward difference approximation is applied in contact positions $\{n-2, n-1\}$

$$\omega_{1,j} = \frac{3\phi_{1,j} - 4\phi_{1,j-1} + \phi_{1,j-2}}{2\Delta t} \tag{8}$$

4. The input power is computed at each contact position j as

$$H_{\text{input},j} = T_1\omega_{1,j} \tag{9}$$

5. At each contacting node i of the finite element model, two magnitudes are retrieved from the finite element analysis at each contact position j, the tangential force $\mathbf{F}_{j,i}$ and the coordinate position under deformation $\mathbf{r}_{j,i}$. The frictional power $H_{\text{loss},j}$ at each contact position j is then determined as

$$H_{\text{loss},j} = \sum_i \mathbf{F}_{j,i} \cdot \left[\boldsymbol{\omega}_2 \times (\overrightarrow{O_2O_1} + \mathbf{r}_{j,i}) - \boldsymbol{\omega}_{1,j} \times \mathbf{r}_{j,i}\right]$$

6. The power loss $H_{\text{loss},j}$ at each contact position j can be also determined from the output power $H_{\text{output},j}$, which can be calculated from the reaction torque $\mathbf{T}_{2,j}$ at the gear reference node, as

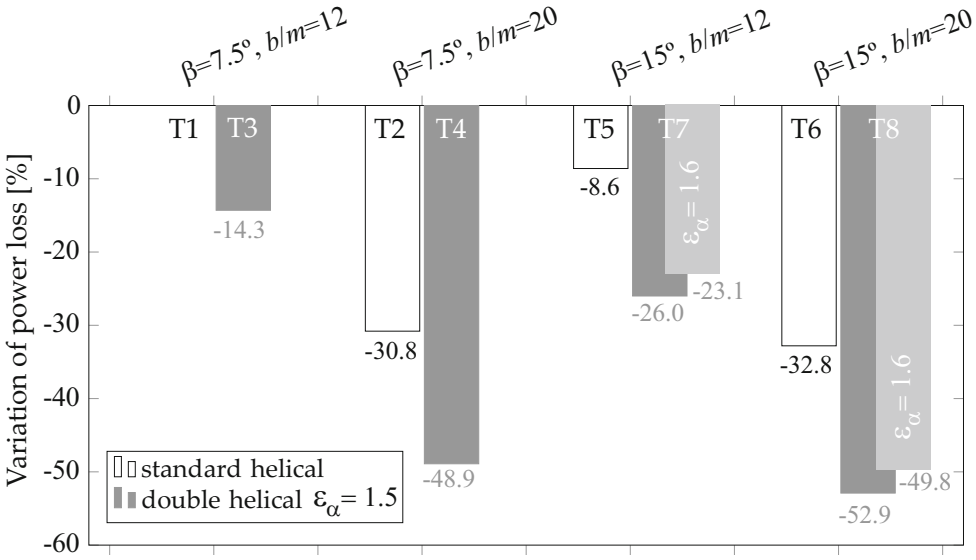

Fig. 12 Variation of power loss with respect to the power loss of transmission T1

$$H_{\text{output},j} = -\mathbf{T}_{2,j} \cdot \boldsymbol{\omega}_2 \tag{11}$$

$$H_{\text{loss},j} = H_{\text{input},j} - H_{\text{output},j} \tag{12}$$

7. The efficiency at each contact position j (instantaneous efficiency) is then computed as

$$\eta_j = \frac{H_{\text{input},j} - H_{\text{loss},j}}{H_{\text{input},j}} \tag{13}$$

8. The mean power loss and the mean efficiency along the cycle of meshing can be derived from the input energy, E_{input}, and the loss energy, E_{loss}. These energies can be computed from their corresponding powers by numerical integration. Applying Simpson rule 1/3 and assuming an odd number for n [13]:

$$\vee\, k = \{1, ..., (n-1)/2\} \longrightarrow j = 2k - 1$$

$$E_{\text{input}} = \sum_k \frac{1}{3}(H_{\text{input},j-1} + 4H_{\text{input},j} + H_{\text{input},j+1})\Delta t$$

$$E_{\text{loss}} = \sum_k \frac{1}{3}(H_{\text{loss},j-1} + 4H_{\text{loss},j} + H_{\text{loss},j+1})\Delta t$$

$$H_{\text{loss,mean}} = \frac{E_{\text{loss}}}{\Delta t(n-1)} \tag{14}$$

$$\eta_{\text{mean}} = \frac{E_{\text{input}} - E_{\text{loss}}}{E_{\text{input}}} \tag{15}$$

6 Results

A total of eight two-stage gear transmissions are being compared in terms of efficiency. Each gear transmission is associated to a different type of helical gear. Four types of gears are shown in Fig. 7, considering two facewidth-to-module ratios, $b/m \approx 12$ and $b/m \approx 20$, and single standard configuration versus double staggered helical configuration. At

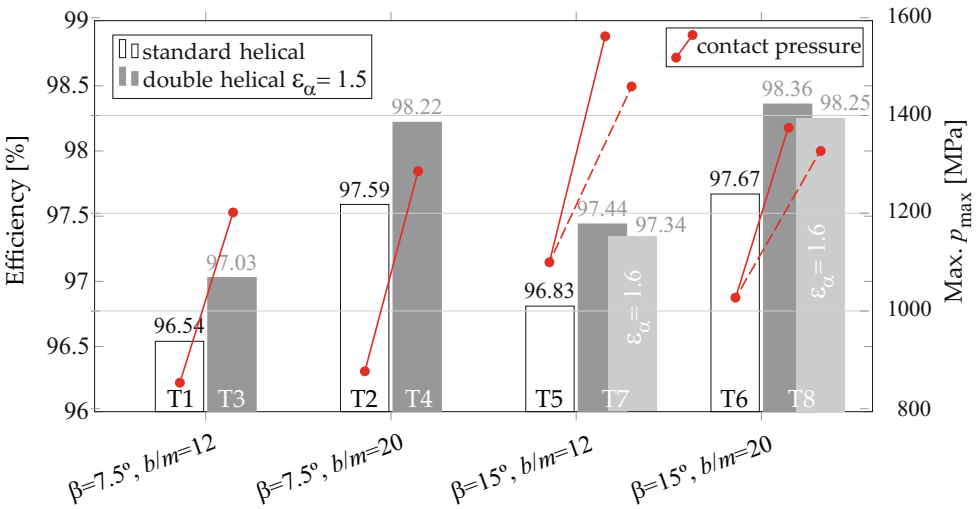

Fig. 13 Efficiencies of the eight two-stage gear transmissions and maximum value of the evolution of p_{max}

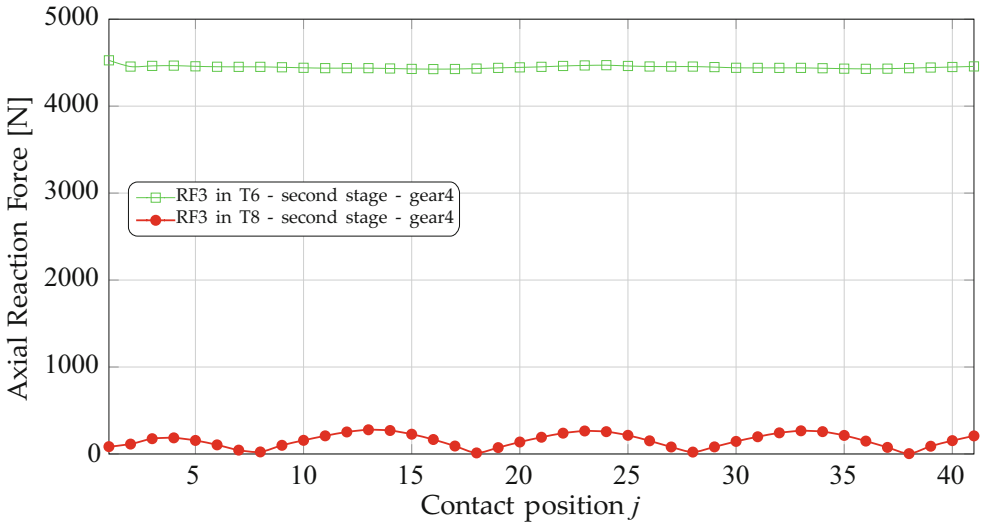

Fig. 14 Axial reaction force at gear reference node of the stage 2 of transmissions T6 (based on standard helical gears) and T8 (based on double staggered helical gears with shortened teeth)

each type, two helix angles of 7.5° and 15.0° are being considered as well.

The input power and input torque are common to all the gear transmissions: 60 kW and 137 Nm. A reference gear ratio of 9.6 is considered as well for all the transmissions. Application of AGMA901-A92 [14] allows to split the gear ratio in 3.3 and 2.9 for the first and the second stage, respectively. These gear ratios are considered as references in the design of each stage, which may allow a variation of 5% of the gear ratio. Table 1 shows the design variables of the eight two-stage gear transmissions, where T1, T3, T5 and T7 have $b/m \approx 12$ and T2, T4, T6 and T8 have $b/m \approx 20$. A normal pressure angle of 20° and a root radius coefficient of 0.38 are considered in all the designs. The material for all the gears is hardened steel 18CrNiMo7-6 and the required service life is 20000 hours. A maximum torque per unit weight is set as an objective goal in the transmissions with standard helical gears (T1, T2, T5 and T6), with observation of a flank safety $S_H > 1.0$ [15]. Transmissions with double staggered helical gears (T3, T4, T7 and T8) are obtained from their counterpart transmissions with standard helical gears using short addendum and dedendum to get a transverse contact ratio $\varepsilon_{\alpha,d} = 1.5$. Any other value of the transverse contact ratio may be fixed by the designer to get a compromise solution between an allowable maximum contact pressure and an increased efficiency.

Fig. 8 shows schematically two of the eight transmissions. Only the gears are represented in Fig. 8 for the purpose of clarity.

For each stage of every transmission, optimized tip and root reliefs are found for the pinion tooth surfaces, providing a minimum value of the maximum contact pressure along the cycle of meshing. A finite element model is built for each transmission stage. For example, the finite element model for stage 1 of transmission T1 has a total of 220 224 nodes with 181 500 elements. Brick elements of eight nodes C3D8I [12] are considered. This model is provided with five pairs of contacting teeth and is similar to the one illustrated in Fig. 5, but without the incision part. A torque $T_1 = 137$ Nm is applied to the pinion reference node. Fig. 9a shows the evolution of the contact pressure along 41 contact positions of the cycle of meshing in the five pairs of contacting teeth when a tip-root relief with $l_a = l_f = 1.5$ mm and $C_{\alpha a} = C_{\alpha f} = 7\,\mu$m is considered (see Fig. 3). At each contact position j, the maximum value of contact pressure, $p_{\max}$, is obtained. The maximum value of $p_{\max}$ for this case is 816.13 MPa at contact position $j = 23$ as it is illustrated in Fig. 9a. Fig. 9b shows a comparison of the evolution of $p_{\max}$ when different values of tip-root relief $C_{\alpha a} = C_{\alpha f}$ are considered for the same fixed value $l_a = l_f = 1.5$ mm, providing the optimized evolution of $p_{\max}$ for 7.0 μm.

Table 2 shows the optimized tip-root relief and the maximum value of the optimized evolution of $p_{\max}$ for each stage and transmission. Transmissions with double staggered helical gears and shortened teeth (transmissions T3, T4, T7 and T8) show an increment of the contact pressure with respect to standard helical gears, and consequently, a decrement in the flank safety. Here, the minimum flank safety is computed from the effective allowable contact stress number obtained from application of Standard AGMA 2001-D04 [15] to the pinion (1300 MPa for stages 1 and 1335 MPa for stages 2) and the value of the maximum contact pressure obtained from the finite element analyses.

The transmissions with the optimized tip-root relief are then analyzed considering friction. The same constant friction coefficient is assumed in all the transmissions, which are supposed to be made of steel and are all well lubricated. Although the friction coefficient depends on many factors, such as the type of material, the sliding velocities, thermal effects, lubrication and ambient conditions among others,

a constant value $\mu = 0.08$ will be considered here for the purpose of comparing the geometry effect.

Fig. 10 shows the input and output powers, the power loss obtained from Eq. (10) and from Eq. (12), the instantaneous efficiency (see Eq. (13)) and the mean efficiency (see Eq. (15)) for the Stage 1 of transmission T1, using $\mu = 0.08$. Fig. 11 shows the same type of results but for the Stage 1 of transmission T3. Both figures show how the double staggered helical gears with shortened teeth reduce the amplitude of variation of the power loss, reducing the mean power loss from 949.9 W to 806 W, which means an increment in 0.3 points in the mean efficiency of Stage 1.

Table 3 shows the computed mean power losses $H^{(1)}_{\text{loss,mean}}$ and $H^{(2)}_{\text{loss,mean}}$ (see Eq. (14)) corresponding to Stages 1 and 2, respectively, at each transmission. The efficiencies at each transmission are as well illustrated as the product of the mean efficiencies, computed at each stage as $\eta^{(1)}_{\text{mean}}$ and $\eta^{(2)}_{\text{mean}}$ through Eq. (15).

The variations of power loss with respect to the power loss of transmission T1 are represented in Fig. 12. It can be observed that the reduction of power loss by using a larger facewidth-to-module ratio is larger than the reduction by using double staggered helical gears with shortened teeth. However, the two effects simultaneously applied, a larger facewidth-to-module ratio and the use of double staggered helical gears with shortened teeth, result in a even larger reduction of the power loss. It is also observed that the use of a larger helix angle has no too much effect, specially when the two above mentioned effects are applied. Fig. 12 shows as well the effect of increasing the contact ratio in transmissions T7 and T8 from 1.5 to 1.6.

The computed efficiency at each transmission is also illustrated in Fig. 13 for a better comparison. Fig. 13 shows an increment in the efficiency of transmissions T3, T4, T7 and T8 (using double staggered helical gears with shortened teeth) with respect to transmissions T1, T2, T5 and T6 (using standard helical gears). Fig. 13 illustrates also that the use of a larger facewidth to module ratio increases the efficiency as it can be drawn from comparisons T1-T2, T3-T4, T5-T6, T7-T8. Fig. 13 shows that the use of a helix angle of 15° has just a slight advantage respect to a helix angle of 7.5°. Besides the efficiency results, Fig. 13 also shows the maximum value of the contact pressure found at each transmission (it can belong to Stage 1 or to Stage 2). It can be seen that the use of double staggered helical gears with short addendum and dedendum involves an increment of the contact pressure, which will depend on the selected transverse contact ratio.

Finally, the variation of the axial reaction force in double staggered helical gears with shortened teeth has been investigated. Fig. 14 shows a comparison of the reaction force along the axial axis at the gear reference node of stage 2 in transmissions T6 (based on standard helical gears) and T8 (based on double staggered helical gears with shortened teeth). Fig. 14 shows a fluctuation approximately between 0 N and 280 N of the axial reaction force in gear 4 of transmission T8.

7 Conclusions

The performed research allows the following conclusions to be drawn:

1. The power loss of a gear drive has been determined from the finite element analysis results using two methods of computation (see Eq.(10) and Eq.(12)) and showing very similar results. Both methods use a constant friction coefficient and provide a mean efficiency based on the computation of the frictional energy along the cycle of meshing. So, the calculation of the efficiency is based just on the computation of load-dependent power loss.
2. The use of double staggered helical gears with half angular pitch offset between their parts and short addendum and dedendum implies a reduction of the load-dependent power loss respect to the use of standard helical gears in gear drives with similar transverse contact ratio. The reduction affects not only to the mean value of the power loss but also to the amplitude of variation of the instantaneous power loss along the cycle of meshing.
3. The use of double staggered helical gears with shortened teeth and the use of larger facewidth to module ratios provide accumulative effects to reduce the power loss and increase the efficiency. However, the use of larger helix angles hardly have effects in the increment of the efficiency. For the analyzed two-stage transmissions, the results show an increment in 1.8 percentile points in the mean efficiency of the highest one with respect to the lowest one.
4. The use of double staggered helical gears with short addendum and dedendum implies an increment of the contact pressure. Such an increment may represent a drawback in some cases and may lead to apply a larger transverse contact ratio (increasing the addendum and dedendum) and consequently to reduce the improvement in the efficiency.
5. Double staggered helical gears cause a slight variation of the axial reaction force along the cycle of meshing. Its magnitude is negligible respect to standard helical gears and perfectly acceptable.

Funding This publication is part of the research project PID2020-116107GB-I00 funded by MCIN/AEI/10.13039/501100011033. Open Access funding provided thanks to the CRUE-CSIC agreement with Springer Nature.

Conflict of interest On behalf of all authors, the corresponding author states that there is no conflict of interest.

References

1. Stadtfeld HJ (2020) Introduction to electric vehicle transmissions. Gear Technol 37(7):42–50
2. Concli F (2017) Low-loss gears precision planetary gearboxes: reduction of the load dependent power losses and efficiency estimation through a hybrid analytical-numerical optimization tool. Forsch Ingenieurwes 81:395–407. https://doi.org/10.1007/s10010-017-0242-0
3. Sheng W, Li Z, Zhang H, Zhu R (2021) Geometry and design of spur gear drive associated with low sliding ratio. Adv Mech Eng. https://doi.org/10.1177/16878140211012547
4. Farrenkopf F, Schwarz A, Lohner T, Stahl K (2022) Analysis of a low-loss gear geometry using a thermal elastohydrodynamic simulation including mixed lubrication. Lubricants. https://doi.org/10.3390/lubricants10090200
5. Xu H, Kahraman A, Anderson NE, Maddock DG (2007) Prediction of mechanical efficiency of parallel-axis gear pairs. J Mech Des 129:58–68. https://doi.org/10.1115/1.2359478
6. Kolivand M, Li S, Kahraman A (2010) Prediction of mechanical gear mesh efficiency of hypoid gear pairs. Mech Mach Theory 45:1568–1582. https://doi.org/10.1016/j.mechmachtheory.2010.06.015
7. Baglioni S, Cianetti F, Landi L (2012) Influence of the addendum modification on spur gear efficiency. Mech Mach Theory 49:216–233. https://doi.org/10.1016/j.mechmachtheory.2011.10.007
8. Arana A, Larrañaga J, Ulacia I (2019) Partial EHL friction coefficient model to predict power losses in cylindrical gears. Proc Inst Mech Eng Part J: J Eng Tribol 233:303–316. https://doi.org/10.1177/1350650118778655
9. Roda-Casanova V, Gonzalez-Perez I (2021) Investigation of the effect of contact pattern design on the mechanical and thermal behaviors of plastic-steel helical gear drives. Mech Mach Theory. https://doi.org/10.1016/j.mechmachtheory.2021.104401
10. Litvin FL, Fuentes A (2004) Gear geometry and applied theory. Cambridge University Press
11. Piegl L, Tiller W (1996) The NURBS book. Springer, Berlin, Heidelberg
12. Dassault Systemes Simulia Corp. (2015) Abaqus theory guide. Dassault Systemes
13. Jaluria Y (1996) Computer methods for engineering. Taylor & Francis
14. American Gear Manufacturers Association (1992) AGMA 901-A92: A rational procedure for the preliminary design of minimum volume gears
15. American Gear Manufacturers Association (2016) AGMA 2001-D04: Fundamental rating factors and calculation methods for involute spur and helical gear teeth